Heliyon 10 (2024) e37949

Contents lists available at ScienceDirect

Heliyon

journal homepage: www.cell.com/heliyon

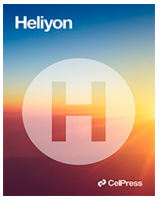

Research article

High-performance adsorption of methylene blue using novel bio-adsorbent based on sargassum fusiforme

Zhutao Long, Zicheng Wang, Qiong Huang, Yulei Jia, Zhiyong Jiao, Yudou Wang, Yonggang Du *

College of Science, China University of Petroleum (East China), Qingdao, Shandong, 266580, China

ARTICLE INFO

Keywords:
Sargassum fusiforme
Adsorption
Methylene blue
High-performance
Bio-adsorbent

ABSTRACT

Large specific surface area obtained by pyrolyzed biomass is considered as a vital factor in improving the dye adsorption performance. However, pyrolysis would cause the inevitable destruction of the surface functional groups of biomass. Herein, a biomass adsorbent based on sargassum fusiforme without pyrolysis was employed for the removal of methylene blue (MB). Combining the FTIR, XPS, SEM, and BET analysis, sargassum fusiforme bio-adsorbent (SFBA) was found to have low specific surface area whereas rich functional groups, including carboxyl, carbonyl and hydroxyl groups. SFBA presented high adsorption performance towards MB with a maximum adsorption capacity of 1154.05 mg/g, demonstrating that the high adsorption performance could be achieved by abundant functional groups rather than large specific surface area. In this paper, various adsorption parameters including pH, concentration, contact time, and temperature have also been discussed. The results indicated that the kinetic and isotherm models of SFBA followed the pseudo-secondary kinetic model and the Langmuir isotherm model, respectively. The negative thermodynamic parameters showed that the adsorption process is spontaneous and exothermic. The SFBA enriched with functional groups exhibited high adsorption performance as well as simple fabrication, and abundant sources that could provide a novel alternative for the treatment of dye wastewater.

1. Introduction

Water pollution is a serious issue in the world due to the inevitable discharge of dye wastewater from textile, leather, printing dyeing, dye manufacturing and other industries [1]. As per available data, there are over 100,000 dyes used in these industries worldwide, of which methylene blue (MB) is a typical cationic dye with complex aromatic structure [2]. Owing to its stability, difficulty in degradation, toxicity and carcinogenicity, the discharge of MB not only causes serious damage to the ecological environment [3], but also poses a present or potential hazard to human health [4]. Hence, the removal and decomposition of MB from wastewater bear great significance. Currently, the main removal methods adopted to treat wastewater include membrane filtration [5], reverse osmosis [6], advanced oxidation [7] and adsorption [8] etc., among which, adsorption is considered to be the most promising method in light of its simplicity, efficiency, no secondary pollution and low cost [9]. However, there are a wide disparity in the adsorption performance and fabrication process of various adsorbent materials due to their different physical and chemical properties. Therefore,

* Corresponding author.
E-mail address: duyg@upc.edu.cn (Y. Du).

https://doi.org/10.1016/j.heliyon.2024.e37949
Received 20 February 2024; Received in revised form 7 September 2024; Accepted 13 September 2024
Available online 16 September 2024

the development of high-performance whereas easy to fabricated adsorbents is crucial.

To date, researchers have investigated the adsorption of MB employing nanocomposite [10], hydrogels [11] and biochar [12] as adsorbents. Among them, nanocomposite and hydrogel have high adsorption properties but the challenges in terms of complex preparation processes and low yields due to the relative scarcity of raw materials, which limit their practical application in large-scale water treatment. Biochar is a solid material obtained by pyrolyzing biomass with abundant raw materials in an anaerobic environment [13], whose large specific surface area and high porosity produced by pyrolysis are broadly considered as vital factors in its adsorption capacity [14]. In this context, researchers have focused on enhancing the specific surface area and porosity of the adsorbent by pyrolysis of various biomasses into biochar to improve the adsorption capacity [15]. However, the maximum adsorption capacity of MB on biochar prepared from biomass such as seaweed, sewage sludge, rice straw and other agricultural wastes ranges from roughly 20–500 mg/g [16–20], which is still unsatisfactory for practical applications. Besides, the pyrolysis process requires high temperature, which leads to high energy consumption and thus increases the cost, and more notably, some functional groups of the biomass that are critical for adsorption are destroyed resulting their role in adsorption wholly or partially lost [21]. In order to improve the adsorption capacity of biochar, some researchers have specially introduced functional groups by chemical modification into biochar. For example, S. Liu et al. succeeded to introduce oxygen-containing groups onto the banana pseudostem biochar surface with phosphomolybdic acid modification and the MB adsorption capability was enhanced from 87.28 mg/g to 146.23 mg/g [22]. Y. Zhang et al. enhanced the hydroxyl and carboxyl groups on the surfaces of ball-milled hickory chip biochar by hydrogen peroxide modification, which increased its MB adsorption capacity by 1.7 times, up to 310 mg/g [23]. Accordingly, the development of low-cost adsorbents with high adsorption capacity, simple fabrication, low energy consumption and abundant sources seems to be able to strive in the direction of biomass containing abundant functional groups [24].

Seaweed is an attractive green and renewable biological resource, with over 1000 species of seaweed growing in aquatic environments. It has been reported that algal biomasses have shown the potential to remove dyes, probably due to the presence of active functional groups such as hydroxyl, carboxyl, carbonyl, amine, and sulfate [25]. For example, a study was conducted by S. El Atouani et al. on the adsorption of MB using Sargassum muticum biomass with a maximum adsorption capacity of 191.38 mg/g [26]. K. Marungrueng et al. have reported the adsorption of MB by green macroalga Caulerpa lentillifera biomass, achieving a maximum adsorption capacity of 417 mg/g [27]. The sargassum fusiforme is a type of brown algae widely distributed in the coastal areas of the Yellow Sea and Bohai Sea in China, and has been used in medical research due to its bioactive polysaccharides with antitumor, immunomodulatory, anti-hyperlipidemia and antioxidant [28]. Nevertheless, its adsorption properties to dyes contaminants such as MB have not been explored yet. In this study, the batch adsorption study of MB employing sargassum fusiforme as a bio-adsorbent is presented. Interestingly, it is different from the conventional belief that only pyrolysis or complex fabrication can improve the adsorption performance of biomass, sargassum fusiforme that requires no handling whatsoever has outstanding properties for removing MB, with a maximum adsorption capacity of 1154.05 mg/g.

The main objective of this work is to propose and investigate the adsorption performance and adsorption mechanism of sargassum fusiforme bio-adsorbent (SFBA) towards MB. Characterizations of SFBA were carried out by Fourier transmission infrared spectroscopy (FTIR), Scanning electron microscopy (SEM), X-ray photoelectron spectroscopy analysis (XPS), Brunauer-Emmett-Teller analysis (BET) and Thermogravimetric analysis (TGA). The adsorption kinetics, adsorption isotherms and adsorption thermodynamics on the

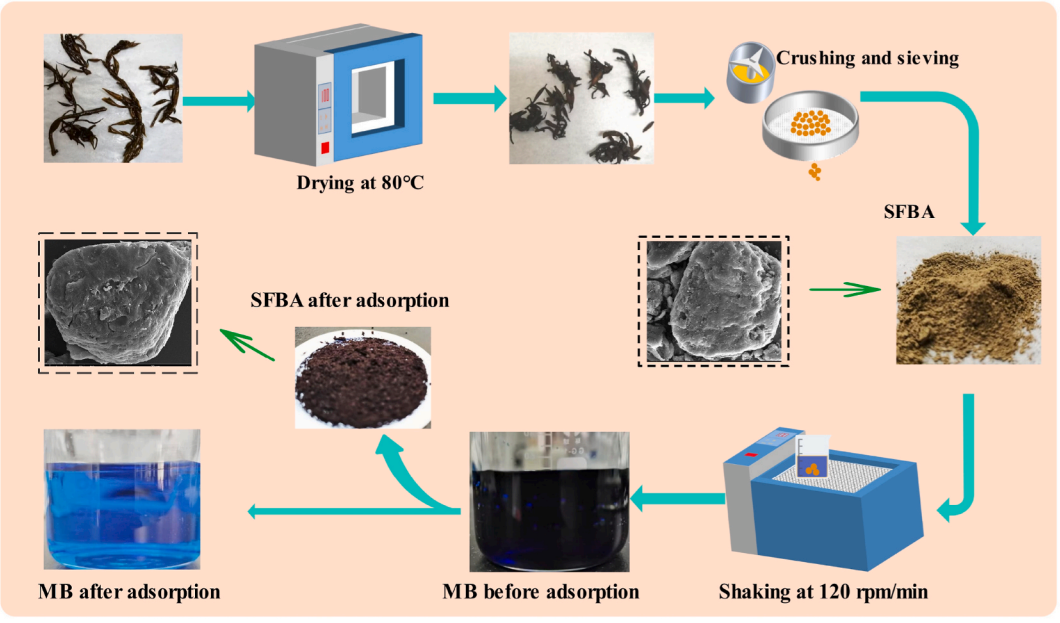

Fig. 1. Schematic diagram of the preparation process of SFBA.

adsorption behavior were studied in batch. Moreover, the reusability performance of SFBA was evaluated. It is concluded that the SFBA developed in this paper is a very promising high-performance and low-cost wastewater adsorbent for practical application.

2. Materials and methods

2.1. Materials

The sargassum fusiforme used was produced in Liaoning, China. MB ($C_{16}H_{18}ClN_3S$) was obtained from Tianjin Guangcheng Chemical Reagent Company Limited (Tianjin, China). Hydrochloric acid (HCl, AR) was purchased from Sinopharm Chemical Reagent Company Limited (Shanghai, China). Sodium hydroxide (NaOH, AR) was purchased by Xilong Science Company Limited (Shantou, China). A series of different concentrations of MB solutions were prepared using deionized water. All chemicals and solvents used in this study were of analytical grade.

2.2. Fabrication of SFBA

The fabrication of SFBA features simplicity, economy and eco-friendliness. The collected sargassum fusiforme were first washed 4–5 times with deionized water and then dried in a vacuum drying oven (DZF, Beijing Yong Guangming Medical Instrument Ltd, China) at 80 °C for 8 h to obtain a constant weight. The dried samples were crushed and sieved at 150 mesh with a homogeneous size of SFBA, and finally, the resulting sorbent powder was packed into vials and sealed for subsequent sorption experiments. The specific experimental flow diagram is shown in Fig. 1.

2.3. Characterization of SFBA

FTIR analysis was performed using an infrared spectrometer (Thermo Scientific Nicolet IS50, USA) in the frequency range of 400–4000 cm^{-1} with 4 cm^{-1} resolution and at room temperature. The surface characteristics and morphology of SFBA were observed by SEM (FEI NovananoSEM450, USA), with gold spraying applied to the sample surface prior to SEM visualization, and the elemental composition of the adsorbent surface was examined by EDS (Oxford Inca Energy X-max-50, UK). XPS (Thermo escalab250Xi, USA) was used to detect the elemental composition and high-resolution spectra of C 1s, and all XPS spectra were acquired using the Al Kα emission. The specific surface area and pore size were determined by BET (Micromeritics ASAP 2460, USA) using N_2 as the adsorption gas and the result shown in Fig. S1. TGA was carried out using TG-DTA (NetzschTG209F3, Germany) at a ramp-up temperature of 30–600 °C and a ramp-down rate of 10 °C/min, maintaining a nitrogen atmosphere throughout. The samples used for characterization were all dried in a vacuum drying oven before characterization.

2.4. MB adsorption

A series of experiments were performed to evaluate the adsorption behavior of SFBA towards MB, which included measurements of pH, initial concentration, contact time and adsorption temperature of MB on adsorption performance. For the kinetic studies, 0.3 g of SFBA was added to 500 mL of 100 mg/L, 500 mg/L, 900 mg/L MB solution and shaken (120 rpm/min, 25 °C) in a constant temperature water bath shaker (SHA-A, Jinan Wolong Experimental Instruments Company Limited, China), then supernatant were taken at different time intervals and the residual dye concentrations of the supernatant were measured at 664 nm using a UV spectrometer (UV-2600, Shimadzu, Japan). The adsorption capacity q_e(mg /g) was calculated using equation (1).

$$q_e = \frac{(C_0 - C_e)V}{M} \tag{1}$$

$$R_e = \frac{(C_o - C_e)}{C_o} \times 100 \tag{2}$$

Where C_0(mg /L) and C_e(mg /L) denote the concentration of MB before and after

the adsorption experiment, respectively. V(L) denotes the volume of the solution and M(g) denotes the mass of the added SFBA. To investigate the optimal adsorption concentration and adsorption isotherm, 0.03 g of SFBA was added to 50 mL of 5–1500 mg/ L MB solution and shaken (120 rpm/min, 25 °C) in a constant temperature water bath shaker, and then repeat the experiment at 35 and 45 °C. The beaker was shaken in a constant temperature water bath shaker for 8 h, and the supernatant was taken to measure the equilibrium concentration of MB after reaching adsorption equilibrium. The adsorption thermodynamics was further investigated by data from adsorption isotherm measurements. In addition, the point of zero charge (pH_{pzc}) of SFBA was determined in this study [29]. MB solution with pH ranging from 2 to 12 was configured with 0.1 M HCL and NaOH. MB solution (50 mL, 100 mg/L) of different pH was adsorbed with 0.03 g SFBA and the pH of the solution was measured after reaching adsorption equilibrium. ΔpH is the difference in pH before and after adsorption and the point of zero charge is the pH value at ΔpH = 0. The effect of varying the pH from 2 to 10 on the adsorption capacity and removal efficiency (R_e) of MB was also studied at 25 °C. The removal efficiency was calculated by equation (2).

2.5. Desorption experiment and reusability

The reusability experiment was conducted in two steps. Firstly, 0.3 g of SFBA was added to MB solution (500 mL, 500 mg/L) to bring it to adsorption equilibrium. Next, the MB-loaded SFBA was desorbed with 0.1 M HCl for 3 h [30], then the desorbed SFBA was eluted to neutrality with NaOH and distilled water. After drying, the regenerated SFBA was used to continue adsorption of 500 mg/L of MB solution. Repeating the above adsorption-desorption process four times, the reusability of the SFBA was evaluated by measuring adsorption capacity of the adsorbed solution.

3. Results and discussion

3.1. Characterization of SFBA

3.1.1. FTIR analysis

The FTIR spectra of SFBA before and after adsorption and regeneration of the peaks are shown in Fig. 2. The broad absorption peak at 3372 cm^{-1} is related to the stretching vibration of O-H [31]. Peaks at 2928 cm^{-1} and 1420 cm^{-1} represent the stretching vibration and symmetric bending of C-H, respectively [32,33]. The characteristic band at 1619 cm^{-1} is attributed to the C=O in carboxylic acids with intermolecular hydrogen bonds and 1258 cm^{-1} corresponds to the presence of a sulfur group, possibly due to the presence of fucoidan component in SFBA [34]. The stretching vibrations of C-O in carboxylic acids and the bending vibrations of C-H in aromatic hydrocarbons located at the wavenumber of 1034 and 819 cm^{-1}, respectively [35].The above results indicate that the surface of SFBA contains a mass of carboxyl, carbonyl and hydroxyl groups, which may be potential active sites for interaction with cationic dyes. By comparing the FTIR spectra before and after adsorption, it can be obtained that the peaks of the stretching vibrations of O-H, C=O and C-O moved from 3372, 1619 and 1034 to 3373, 1598 and 1036 cm^{-1} respectively after adsorption, which indicates that these functional groups are indeed involved in the process of MB adsorption by SFBA [36]. Besides, the FITR spectra after adsorption appeared new peaks at 1489.98, 1390.06, 1248.70 and 884.25 cm^{-1}, which are associated with the skeletal vibration of the dye heterocycle, the symmetric bending vibration of CH_3 and the C-N stretching vibration, indicating that MB had adsorbed on the SFBA [37,38].

3.1.2. SEM-EDS analysis

The surface morphological structure of SFBA was observed by SEM, and the results are shown in Fig. 3. As shown in Fig. 3(a), the surface of SFBA before adsorption is relatively rough, and there are some pore structures of different shapes and sizes, and the particle size is around 30 μm to 50 μm. Fig. 3(b) demonstrates that the surface of the adsorbent after adsorption of MB is relatively smoother, and the surface color is obviously much darker, indicating that MB molecules have been adsorbed in the pores and on the surface of the SFBA [39,40]. The elemental composition of the adsorbent surface is analyzed by EDS. As shown in Fig. 3(c) and (d), the SFBA surface before adsorption contains the most C and O with mass ratios of 49.90 % and 40.44 %, and less N and S with mass ratios of 0 % and 3.81 %, respectively. After adsorption, the C and O contents decreased while the N and S contents increased, with mass ratios of 47.64 %, 29.53 %, 14.17 % and 4.79 %, respectively. This indicates that both C and O are involved in the adsorption process of MB, and the increase in elemental N and S content confirms the adsorption of MB molecules on the adsorbent surface [41].

3.1.3. XPS analysis

The chemical composition on the surfaces of SFBA was further investigated by XPS. The results are shown in Fig. 4(a), where the presence of strong binding energy peaks of C 1s and O 1s and weak binding energy peaks of N 1s and S 2p can be seen, indicating that the main elements of SFBA are C and O with trace amounts of N and S, which is consistent with the previous EDS results. The type of functional group on the surface of SFBA was further analyzed by investigating the high-resolution spectrum of C 1s. As shown in Fig. 4 (b), the highest binding energy peaks on the SFBA surface are C-C, corresponding to at 284.6 eV [42]. In addition, there are also weaker

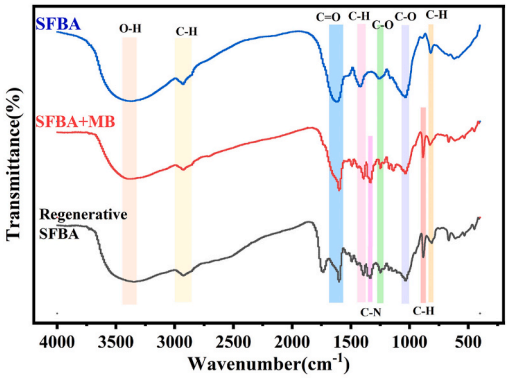

Fig. 2. FTIR spectra of SFBA before and after adsorption and regeneration.

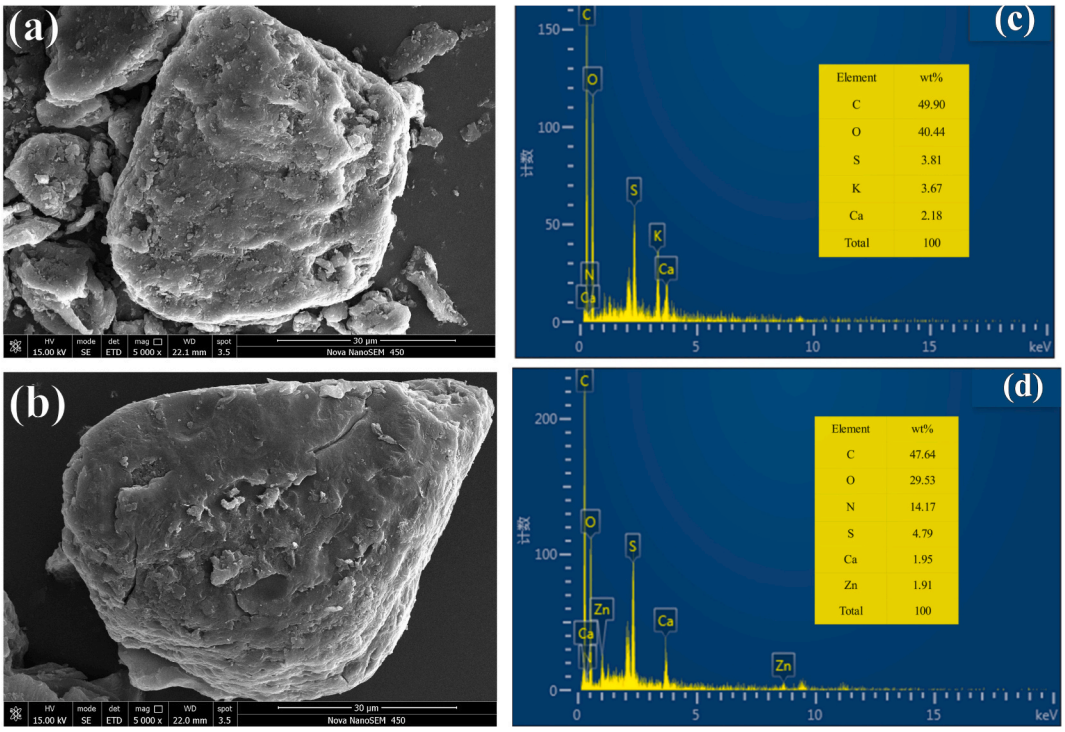

Fig. 3. (a) SEM of SFBA before adsorption, (b) SEM of SFBA after adsorption, (c) EDS of SFBA before adsorption, (d) EDS of SFBA after adsorption.

binding energy peaks for C-O, C=O, and O-C=O at 285.4, 286.25, and 288.4 eV, respectively [43]. Such results are in accordance with the FTIR characterization results.

3.1.4. TGA analysis

The thermal stability of SFBA is analyzed in three parts at temperatures between 30 °C and 600 °C. As shown in Fig. 4(c), the first stage occurs from 55.3 °C to 232 °C with an SFBA mass loss of 9.48 %, corresponding to the evaporation of water and light organic compounds from the adsorbent. The second stage occurs from 232 °C to 340 °C which belongs to the active pyrolysis stage where the weight loss is rapid with a maximum weight loss of 36.25 % which is attributed to the pyrolysis of hemicellulose, cellulose and lipids. The third stage ranges from 340 °C to 597 °C where lignin begins to decompose and weight loss slows down until the final temperature [44]. As above, it can be concluded that SFBA has good thermal stability and its adsorption properties are largely unaffected below 232 °C.

3.2. Effect of initial pH and pH_{pzc} value analysis

The initial pH of the MB solution directly affects the adsorption of MB by SFBA, which is achieved mainly by influencing the degree of ionization of the adsorbate, the level of dissociation of functional groups from the active site and the surface charge with the adsorbent [45]. The effects of pH variation on adsorption capacity and removal efficiency were investigated using MB solution (50 mL, 100 mg/L) with a pH range between 2 and 10. As shown in Fig. 5(a), the adsorption capacity and removal efficiency of SFBA on MB increased remarkably when the initial pH of MB solution increased from 2 to 6, while leveled off when the pH was between 6 and 10, reaching a maximum adsorption capacity of 156.98 mg/g and a maximum removal efficiency of 94.19 % at pH = 10. The observation that the adsorption capacity varies with PH indicates that there is an electrostatic interaction in the adsorption process of SFBA towards MB [37].

The point of zero charge (pH_{pzc}) is an important property to describe the surface charge of the adsorbent. The pH_{pzc} of SFBA can be obtained as 5.62 in Fig. 5(b), and the surface charge of SFBA under this condition behaves as neutral [46]. Under low pH conditions (pH $< pH_{pzc}$), the SFBA surface is positively charged due to the protonation of functional groups, and the excess proton (H^+) will compete with MB cations for adsorption sites, resulting in poor adsorption capacity of SFBA towards MB [37,41]. In contrast, as the solution pH increases, the deprotonation of the adsorbent functional groups is promoted, and the surface charge of SFBA exhibits a negative charge under high pH conditions (pH $> pH_{pzc}$), which is electrostatically attractive to MB cations, thus promoting the adsorption of MB [36].

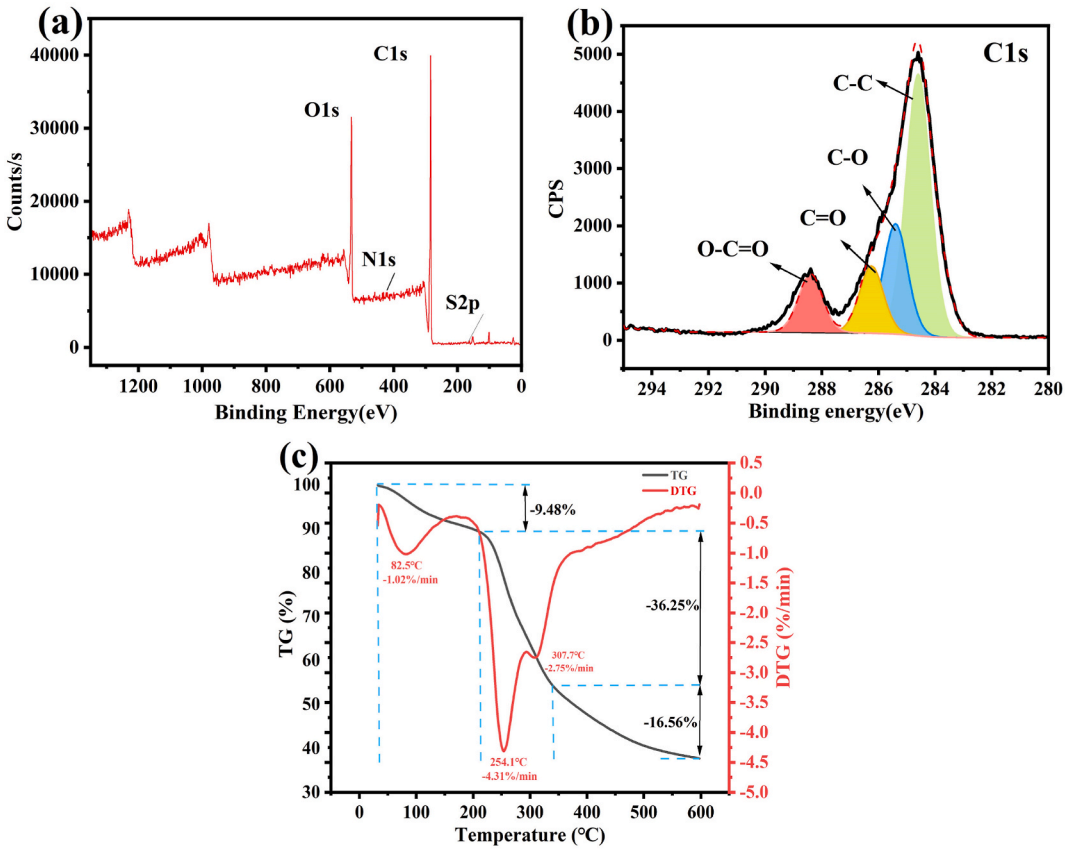

Fig. 4. (a) XPS spectrum of SFBA, (b) C 1s in high resolution spectrum of SFBA, (c) TG-DTG curve.

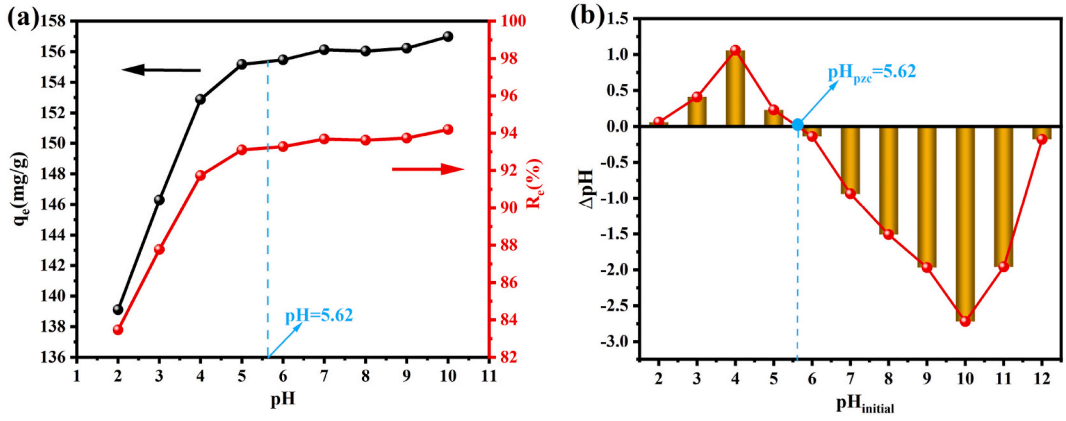

Fig. 5. (a) Effect of initial pH value of MB solution on adsorption capacity and removal efficiency, (b) Zero charge point value of SFBA.

3.3. *Effect of initial MB concentration*

The effects of the initial concentration (5–1500 mg/L) of the MB solution on the adsorption capacity and removal efficiency are displayed in Fig. 6. The adsorption capacity of SFBA towards MB increased gradually with the concentration of MB solution and the adsorption trend plateaued gradually, which is because the driving force of the dye molecules from the aqueous phase to the solid phase increases as the initial concentration of the MB solution increases, overcoming the resistance of the dye molecules to mass transfer between the aqueous and solid phases [35].The gradual plateau of the trend can be attributed to the gradual occupation of the adsorption sites to saturation at higher initial concentrations [47].

The removal efficiency increased and then decreased with the increase of the initial concentration of MB, reaching the maximum

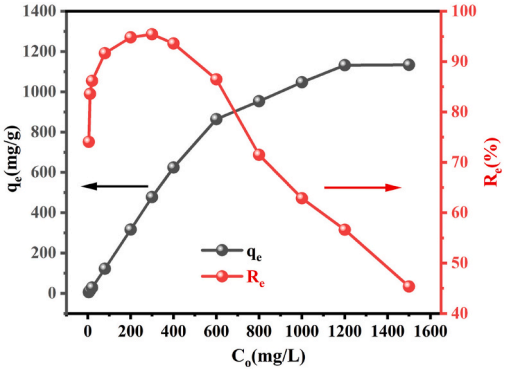

Fig. 6. The plot of the effect of the initial concentration of MB on the adsorption and removal efficiency.

removal rate of 95.44 % at the initial concentration of 300 mg/L and only 45.34 % at the initial concentration of 1500 mg/L. It is due to the high transfer efficiency of MB molecules to vacant sites and the high probability of binding to adsorption sites during the transfer of dye molecules from solution to the SFBA surface as the concentration increased at first [48]. However, after the solute molecules reach optimal uptake, there is a repulsive force between the dye molecules in solution and those in SFBA, such that the removal rate decreases with increasing initial concentration [36].

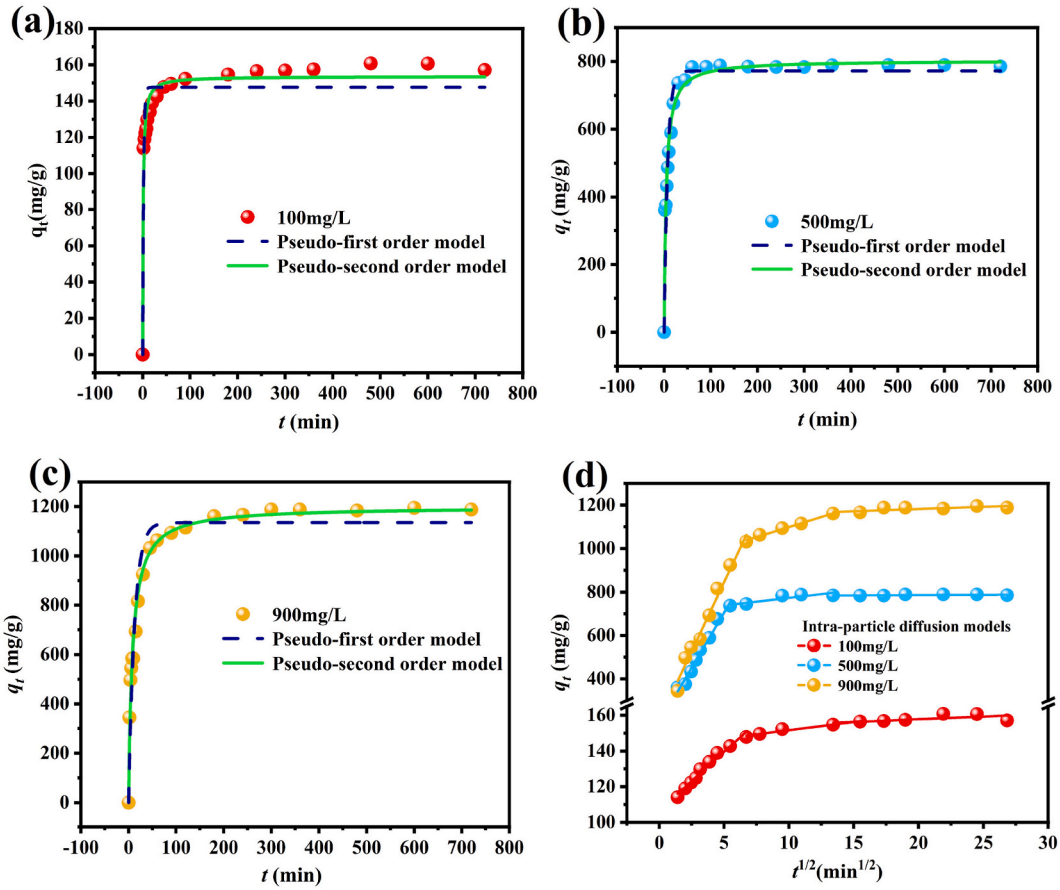

Fig. 7. Plots of kinetic model fitting results for the adsorption of MB by SFBA. (a) Fitted curves of PFO versus PSO at 100 mg/L, (b) Fitted curves of PFO versus PSO at 500 mg/L, (c) Fitted curves of PFO versus PSO at 900 mg/L, (d) Fitted curves of intra-particle diffusion model at different concentrations.

3.4. Adsorption kinetics

In order to analyze the adsorption mechanism from the perspective of adsorption kinetics, the effect of contact time (0–720 min) on the adsorption capacity was investigated using three different concentrations of MB solution (100, 500 and 900 mg/L) and possible rate control steps were explored. The adsorption mechanism depends on the physical or chemical properties of the adsorbent and the mass transfer process [49]. Hence, three common adsorption kinetic models are used to fit the measured experimental data, namely the pseudo-first-order (PFO) kinetic model, the pseudo-second-order (PSO) kinetic model and intra-particle diffusion (IPD) model [50]. The equation expressions for three models are given by equations (3)–(5)

$$q_t = q_e\left(1 - e^{-k_1 t}\right) \tag{3}$$

$$q_t = \frac{k_2 {q_e}^2 t}{1 + k_2 q_e t} \tag{4}$$

$$q_t = k_i t^{\frac{1}{2}} + C \tag{5}$$

where q_e(mg /g) and q_t(mg /g) are the adsorption capacity per unit weight of adsorbent at equilibrium and at t (min), respectively, k_1(1 /min) is the rate constant for the PFO model, k_2(g /(mg · min)) is the rate constant for the PSO model, $k_i\left(\text{mg /g} \cdot \text{min}^{1/2}\right)$ is the rate constant for the IPD model and C (mg/g) is a constant related to the thickness of the boundary layer.

The kinetics fitted curves at three different concentrations are shown in Fig. 7(a–c), it can be seen that the adsorption rate is fast within 10 min and decreases with the increase of adsorption time, and all basically reach the adsorption equilibrium at 240 min. The kinetic parameters obtained by fitting the PFO and PSO models are shown in Table 1, which shows that the correlation coefficients (R^2) of the PSO model are greater than those of the PFO model, indicating that the adsorption of MB on SFBA is more fitted with the PSO model. By comparing the calculated values of the adsorption capacity (q_e) with the experimental values, it can be seen that the calculated values of the PSO model are in general agreement with the experimental values, which also indicates that the adsorption process of SFBA on MB is highly in line with the PSO model. Therefore, it is known that the rate control step of SFBA towards MB is chemisorption according to the PSO model theory [50]. The adsorption mechanism may be a chemical interaction involving valence electron forces due to exchange or sharing of electrons between the adsorbent and MB molecules [31].

In addition, the experimental data were fitted with an IPD model, for describing the diffusion process of MB molecules inside SFBA. As illustrated in Fig. 7(d), the adsorption of MB on SFBA at different concentrations of MB solution showed a multivariate linear relationship. The adsorption process can be clearly divided into three linear regions with different slopes, and none of the curves penetrates the origin, demonstrating that IPD is not the only rate-controlling step but other mechanisms such as boundary layer mass transfer and chemical interaction also affect the adsorption process [51]. In the first stage, the slope of the linear fitted line is the largest, describing the rapid transfer of MB molecules from solution to the SFBA surface by boundary layer diffusion or external mass transfer effects. The second stage is a gradual adsorption stage with the rate control step of intraparticle diffusion, where the MB molecules gradually diffuse towards the adsorption sites within the SFBA pores. In the third stage, the adsorption capacity is basically stable and the active sites on the inner surface pores are almost completely occupied by MB molecules, reaching adsorption equilibrium [52].

3.5. Adsorption isotherms

The adsorption isotherm is an essential model used to analyze the interaction between the adsorbent and the adsorbate. When the adsorption reaches equilibrium, the adsorption isotherm can reflect the distribution of MB molecules between the solid and liquid phases, which is of significance for the analysis of the adsorption mechanism of MB on SFBA and the maximum adsorption capacity [53]. Herein,the Langmuir, Redlich-Peterson, Freundlich and Temkin isotherm models were employed to investigate the adsorption behavior of SFBA towards MB and to determine the most appropriate isotherm model for adsorption. Four isotherm model equations are as equations (6)–(9) [37]:

$$q_e = \frac{q_m k_l C_e}{1 + k_l C_e} \tag{6}$$

Table 1
Adsorption kinetics parameters of PFO and PSO.

$MB_{initial}$(mg /L)	$q_{e,exp}$(mg /g)	Pseudo-first-order model			Pseudo-second-order model		
		$q_{e1,cal}$	k_1 (min^{-1})	R^2	$q_{e2,cal}$	k_2 ($\text{g·mg}^{-1}\text{·min}^{-1}$)	R^2
100	156.69	147.60	0.5136	0.8913	153.58	0.00570	0.9663
500	788.29	772.15	0.1354	0.9452	792.61	0.00003	0.9780
900	1194.92	1135.07	0.0804	0.9404	1199.55	0.00001	0.9831

$$q_e = \frac{k_{RP} C_e}{1 + \alpha_{RP} C_e^{\,p}} \tag{7}$$

$$q_e = k_F C_e^{\,n} \tag{8}$$

$$q_e = \frac{RT}{b_T} \ln(k_T C_e) \tag{9}$$

$$R_L = \frac{1}{1 + k_l C_o} \tag{10}$$

where q_e(mg /g) represents the equilibrium adsorption capacity, q_m(mg /g) represents the maximum adsorption capacity, C_e(mg /L) represents the equilibrium concentration of MB, k_l(L /mg) is the Langmuir model constant, k_{RP}(L /g) and α_{RP}((mg/L)$^{-p}$) are the Redlich-Peterson model constants, k_F((mg /g) /(mg/L)^n) and n are Freundlich constants, p is a dimensionless exponent, R (8.314 J/mol · K) is the universal gas constant, T (K) is the Kelvin temperature, k_T(L /g) is the Temkin model constant, and b_T(J /mol) is the heat of adsorption. C_o(mg /L) is the maximum initial MB concentration.

Fig. 8(a–d) show the non-linear fits of the adsorption isotherm models for the adsorption of MB on SFBA at 25 °C, 35 °C and 45 °C. The adsorption isotherm parameters are shown in Tables 2 and 3. By comparing the fitted correlation coefficients (R^2) of the four isotherm models, it can be concluded that the adsorption of MB on SFBA is most well suited to the Langmuir model, demonstrating that the adsorption process of SFBA towards MB occurs in the monomolecular layer of the adsorbent and at uniform adsorption sites [41]. Meanwhile, the basic characteristics of the Langmuir isotherm can be described by the dimensionless separation factor R_L as equation (10), with R_L indicating that the Langmuir isotherm is characterized as irreversible ($R_L = 0$), favorable ($0 < R_L < 1$), linear ($R_L = 1$) or unfavorable ($R_L > 1$) [54]. It is clear from the values in Table 2 that the adsorption of MB by SFBA is a favorable process, as they all lie between 0 and 1. Moreover, Table 2 also presents the maximum adsorption capacity is 1154.05 mg/g at 25 °C according to the Langmuir isotherm model, and k_l in Table 2 is the equilibrium adsorption constant, with larger values indicating better adsorption

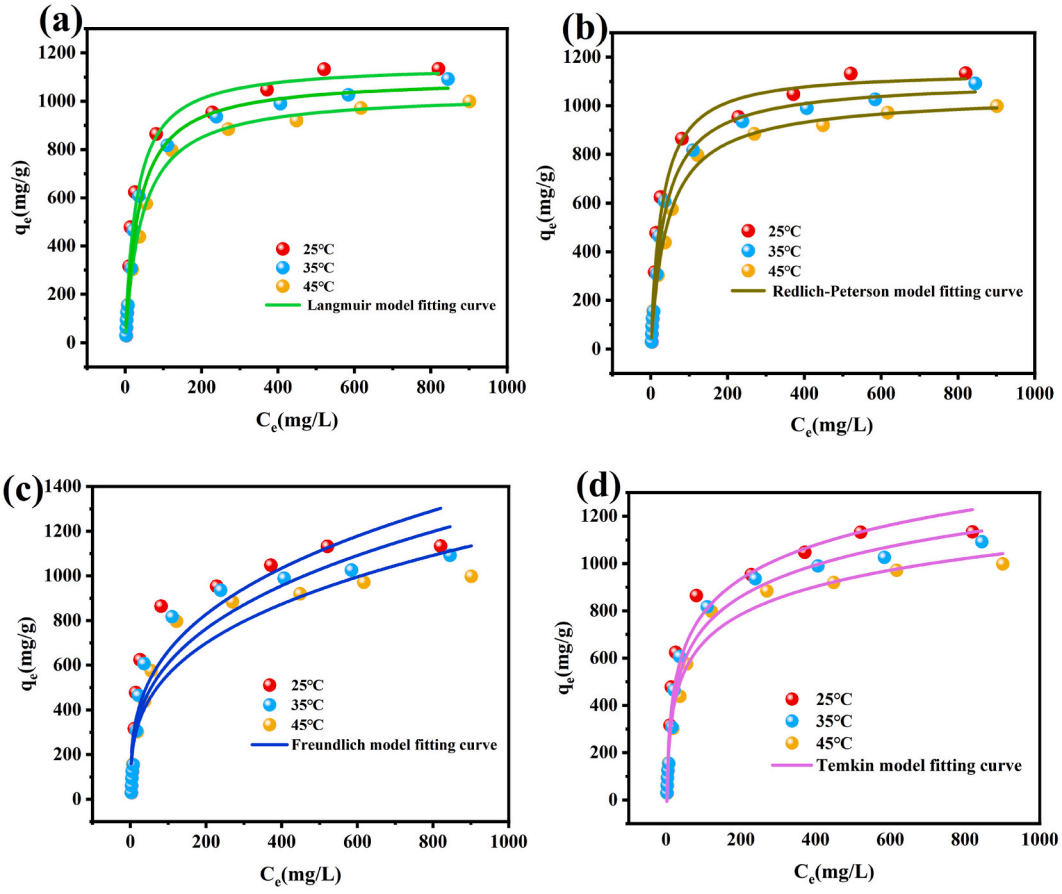

Fig. 8. Fitted isotherm plots for the adsorption of MB on SFBA at different temperatures (25 °C, 35 °C and 45 °C). (a) Langmuir model, (b) Redlich-Peterson model, (c) Freundlich model, (d) Temkin model.

Table 2
Langmuir and Redlich-Peterson constants for the adsorption of SFBA for MB.

Temperature (°C)	Langmuir				Redlich-Peterson			
	q_m (mg/g)	k_l (L/mg)	R^2	R_L	k_{RP} (L/g)	$\alpha_{RP}(mg/L)^{-p}$	p	R^2
25	1154.05	0.0351	0.9778	0.0186	40.0187	0.0333	1.0064	0.9756
35	1097.84	0.0283	0.9930	0.0230	31.4551	0.0296	0.9949	0.9923
45	1034.734	0.0230	0.9964	0.0282	24.4154	0.0252	0.9900	0.9960

Table 3
Freundlich and Temkin constants for the adsorption of SFBA for MB.

Temperature (°C)	Freundlich			Temkin		
	$k_F(mg/g)/(mg/L)^n$	n	R^2	k_T(L/g)	b_T (J/mol)	R^2
25	151.2485	0.3209	0.8844	0.4464	11.9079	0.9731
35	135.8142	0.3258	0.9075	0.4297	13.2633	0.9859
45	126.9883	0.3219	0.9224	0.4893	15.4554	0.9853

[55]. Finally, The equilibrium adsorption constant is the highest at 25 °C, which reveals that the adsorption of MB on SFBA is exothermic.

3.6. Adsorption thermodynamics and effect of temperature

Thermodynamic parameters are an inevitable part of the study of adsorption spontaneity and the adsorption mechanism. In this study, thermodynamic parameters (Gibbs free energy (ΔG^0, KJ/mol), enthalpy change (ΔH^0, KJ/mol) and entropy change (ΔS^0, J/mol · K)) were calculated with experimental data measured at 25 °C, 35 °C and 45 °C. The calculation equations are as follows [56]:

$$\ln K_0 = \frac{\Delta S^0}{R} - \frac{\Delta H^0}{RT} \tag{11}$$

$$\Delta G^0 = -RT \ln K_0 \tag{12}$$

$$K_d = \frac{C_o - C_e}{C_e} \times \frac{V}{m} \tag{13}$$

where K_0 is the equilibrium constant, a is the distribution coefficient, the value of ln K_0 is the intercept of the line fitted by ln K_d against C_e. In addition, R (8.314 J/mol · K) and T (K) represent the ideal gas constant and the solution temperature, respectively. C_o(mg/L) is the initial concentration of MB and C_e(mg/L) is the equilibrium concentration of MB. The values of $-\frac{\Delta H^0}{R}$ and $\frac{\Delta S^0}{R}$ are calculated from the slope and intercept of the curve with ln K_0 versus $1/K$, respectively.

The relationship curve of ln K_0 versus $1/K$ is shown in Fig. 9, and the thermodynamic parameters calculated from the van' t Hoff diagram are shown in Table 4. ΔG^0 is negative at different temperatures, indicating that the adsorption process of SFBA towards MB is

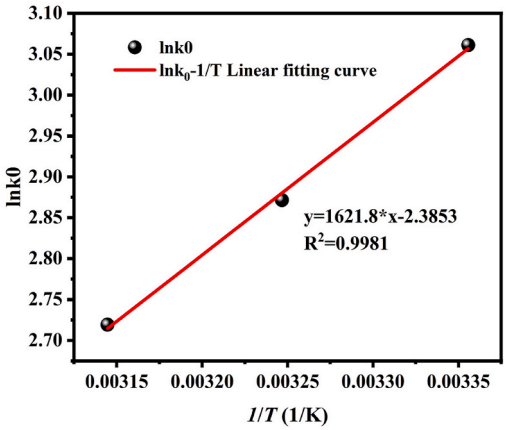

Fig. 9. Plot of ln K_0 versus $1/K$ used to calculate thermodynamic parameters.

Table 4
Thermodynamics constants for the adsorption of SFBA for MB.

Temperature (°C)	ΔG^0 (KJ/mol)	ΔH^0 (KJ/mol)	ΔS^0 (J/mol · K)
25	−7.584	−13.484	−19.831
35	−7.353		
45	−7.189		

spontaneous. As the temperature varies from 45 °C to 25 °C, the absolute value of ΔG^0 becomes larger, indicating that the adsorption process is more spontaneous at room temperature [47], which is also exactly in line with the trend shown in Fig. S3, a more favorable trend for practical applications. The negative value of ΔH^0 (−13.484) once again verifies that the adsorption process of SFBA towards MB is exothermic. The negative value of ΔS^0 (−19.831) means that the randomness of the solid-liquid phase interface is reduced during the adsorption process, facilitating the reordering of the adsorbent surface [45]. Fig. S3 exhibits a decreasing adsorption capacity of SFBA towards MB as the temperature increases. This may be due to the fact that the higher temperature increases the mobility and solubility of MB in solution or leads to an enhancement of the kinetic energy of the components involved in the adsorption, resulting in a weakening of the interaction between the adsorbent and the MB [47].

3.7. Reusability of SFBA

The evaluation of the reusability performance of adsorbents has considerable ecological and economic value for practical applications. The desorption of SFBA loaded with MB was performed using 0.1 M HCl. In combination with SEM and EDS in Fig. S2, the regenerated SFBA surface was found to be crumpled and the N and S mass ratio decreased, indicating that the process of MB desorption from the SFBA surface does exist. As shown in Fig. S4, after the first desorption, the adsorption of MB by SFBA decreased from 772.87 mg/g to 476.63 mg/g. After four cycles, the adsorption capacity of the regenerated SFBA remained more constant at 430.26 mg/g. The above results illustrate that SFBA has reusability properties and is a recyclable bio-adsorbent with potential commercial value.

3.8. Adsorption mechanisms analysis

A schematic diagram of the rational adsorption mechanism of MB in aqueous solutions by SFBA is shown in Fig. 10. There are multiple factors controlling the adsorption process of MB by SFBA, such as the functional groups, pores and active sites on the adsorbent surface, the functional and structural behavior of the adsorbent molecules, etc. According to Fig. 2, the comparison shows that after adsorption, the peaks of O-H, C=O and C-O stretching vibrations moved from 3372, 1619 and 1034 to 3373, 1598 and 1036 cm^{-1} respectively, indicating that the functional groups such as hydroxyl, carbonyl and carboxyl groups present on the surface of SFBA all contribute to the adsorption of MB. The new appeared FITR spectra peak (1489.98, 1390.06 and 1248.70 cm^{-1}) after MB adsorption also reveals that methylene MB had loaded on SFBA surface. The above results suggest that the mechanism of MB adsorption on SFBA may be hydrogen bonding and $n-\pi$ interaction [57]. Further, comparison of the SEM images before and after adsorption displayed that the surface of the adsorbed SFBA is smoother, probably indicating that there are MB molecules filling the pores partly, corresponding results also confirmed by the BET (Fig. S1). Finally, it is found that electrostatic interactions are also an important adsorption mechanism for the adsorption of MB on SFBA by investigating the effect of the initial value of pH on the adsorption capacity and pH_{pzc} value of SFBA.

4. Conclusion

In this study, the adsorption capacity and the adsorption mechanism of SFBA on MB were investigated. The results show that the adsorption of MB on SFBA exhibited pH, initial concentration, contact time and temperature dependent behavior. At pH $>pH_{pzc}$, the best adsorption effect of MB on SFBA is achieved with a maximum removal efficiency of 94.19 %. The adsorption process of MB on SFBA with time follows well the pseudo-second order kinetic model, indicating that the adsorption mechanism is mainly chemisorption. The adsorption process of SFBA towards MB with equilibrium concentration changing is more consistent with the Langmuir isotherm model, and the maximum adsorption amount of SFBA is obtained as 1154.05 mg/g, which shows high adsorption performance due to the presence of abundant functional groups (comparison with biochar from SFBA and other adsorbents are shown in Table S1). The thermodynamic results illustrate that the adsorption of MB on SFBA is a spontaneous exothermic process. Furthermore, after four cycles of adsorption and desorption of MB on SFBA, the adsorption capacity is essentially constant, indicating that SFBA has good regeneration performance. Finally, combining the characterization and experimental results, the adsorption mechanisms of SFBA towards MB include hydrogen bonding, electrostatic interactions, $n-\pi$ interactions and pore filling. In summary, SFBA is a low-cost adsorbent with high adsorption performance, simple process, good regeneration performance, easy availability and no secondary contamination, which provides a novel option for the removal of high concentration organic dyes.

Data availability statement

No data associated with this study has been deposited into a publicly available repository. However, additional raw data can be

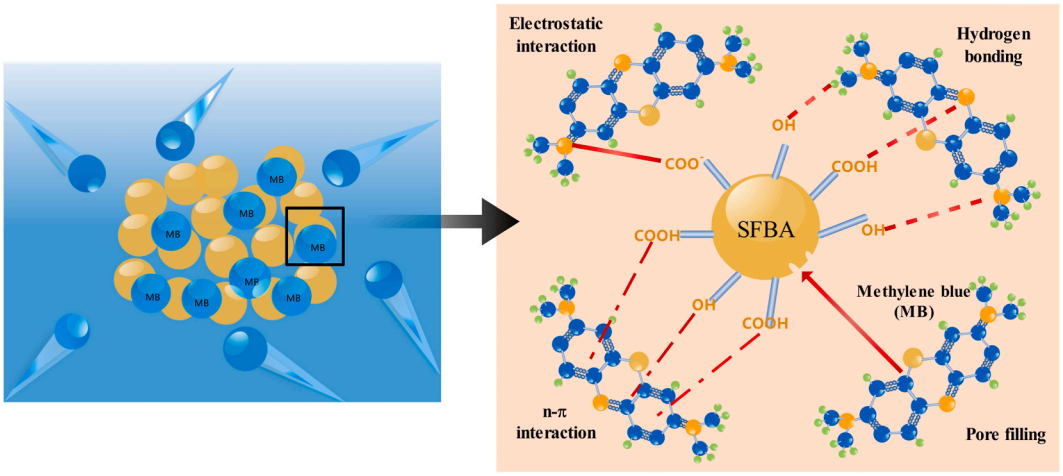

Fig. 10. Diagram of Possible adsorption mechanism of MB on SFBA.

made available on request.

CRediT authorship contribution statement

Zhutao Long: Writing – original draft, Visualization, Methodology, Investigation, Formal analysis, Data curation. **Zicheng Wang:** Methodology, Investigation, Data curation. **Qiong Huang:** Methodology, Investigation, Data curation. **Yulei Jia:** Supervision, Resources, Funding acquisition, Conceptualization. **Zhiyong Jiao:** Supervision, Resources, Funding acquisition. **Yudou Wang:** Methodology, Funding acquisition. **Yonggang Du:** Writing – review & editing, Validation, Supervision, Methodology, Conceptualization.

Declaration of competing interest

The authors declare that they have no known competing financial interests or personal relationships that could have appeared to influence the work reported in this paper.

Acknowledgements

This work was supported by the Key Deployment Project of Ocean Science Research Center of Chinese Academy of Sciences (COMS2020J11), Shandong Province Natural Science Foundation of China (ZR2021ME003) and National Training Program of Innovation and Entrepreneurship for Undergraduates (202111048, 202211045, 202311027CX).

Appendix A. Supplementary data

Supplementary data to this article can be found online at https://doi.org/10.1016/j.heliyon.2024.e37949.

References

[1] P. Sharma, R. Kaur, C. Baskar, W.-J. Chung, Removal of methylene blue from aqueous waste using rice husk and rice husk ash, Desalination 259 (2010) 249–257, https://doi.org/10.1016/j.desal.2010.03.044.
[2] C.J. Mate, S. Mishra, Synthesis of borax cross-linked Jhingan gum hydrogel for remediation of Remazol Brilliant Blue R (RBBR) dye from water: adsorption isotherm, kinetic, thermodynamic and biodegradation studies, Int. J. Biol. Macromol. 151 (2020) 677–690, https://doi.org/10.1016/j.ijbiomac.2020.02.192.
[3] Q. Wang, Y. Wang, L. Chen, A green composite hydrogel based on cellulose and clay as efficient absorbent of colored organic effluent, Carbohydr. Polym. 210 (2019) 314–321, https://doi.org/10.1016/j.carbpol.2019.01.080, 271-278.
[4] S. Shakoor, A. Nasar, Adsorptive decontamination of synthetic wastewater containing crystal violet dye by employing Terminalia arjuna sawdust waste, Groundwater Sustain. Dev. 7 (2018) 30–38, https://doi.org/10.1016/j.gsd.2018.03.004.
[5] H.R. Xiang, X.B. Min, C.J. Tang, M. Sillanpää, F.P. Zhao, Recent advances in membrane filtration for heavy metal removal from wastewater: a mini review, J. Water Process Eng. 49 (2022), https://doi.org/10.1016/j.jwpe.2022.103023.
[6] S.K. Nataraj, K.M. Hosamani, T.M. Aminabhavi, Nanofiltration and reverse osmosis thin film composite membrane module for the removal of dye and salts from the simulated mixtures, Desalination 249 (2009) 12–17, https://doi.org/10.1016/j.desal.2009.06.008.
[7] A.A. Barbosa, R.V.S. de Aquino, N.S. da Cruz Santana Neves, R.F. Dantas, M. Duarte, O. Rossiter Sa da Rocha, Kinetic study of dye removal using TiO_2 supported on polyethylene terephthalate by advanced oxidation processes through neural networks, Water Sci. Technol. 79 (2019) 1134–1143, https://doi.org/10.2166/wst.2019.111.

[8] N. Cheng, B. Wang, P. Wu, X. Lee, Y. Xing, M. Chen, B. Gao, Adsorption of emerging contaminants from water and wastewater by modified biochar: a review, Environ. Pollut. 273 (2021) 116448, https://doi.org/10.1016/j.envpol.2021.116448.

[9] F. Wang, L. Li, J. Iqbal, Z. Yang, Y. Du, Preparation of magnetic chitosan corn straw biochar and its application in adsorption of amaranth dye in aqueous solution, Int. J. Biol. Macromol. 199 (2022) 234–242, https://doi.org/10.1016/j.ijbiomac.2021.12.195.

[10] P.K. Jaseela, J. Garvasis, A. Joseph, Selective adsorption of methylene blue (MB) dye from aqueous mixture of MB and methyl orange (MO) using mesoporous titania (TiO_2)-poly vinyl alcohol (PVA) nanocomposite, J. Mol. Liq. 286 (2019), https://doi.org/10.1016/j.molliq.2019.110908.

[11] O. Duman, T.G. Polat, C.O. Diker, S. Tunc, Agar/kappa-carrageenan composite hydrogel adsorbent for the removal of Methylene Blue from water, Int. J. Biol. Macromol. 160 (2020) 823–835, https://doi.org/10.1016/j.ijbiomac.2020.05.191.

[12] A. Nasrullah, B. Saad, A.H. Bhat, et al., Mangosteen peel waste as a sustainable precursor for high surface area mesoporous activated carbon: characterization and application for methylene blue removal, J. Clean. Prod. 211 (2019) 1190–1200, https://doi.org/10.1016/j.jclepro.2018.11.094.

[13] D. Mohan, A. Sarswat, Y.S. Ok, C.U. Pittman Jr., Organic and inorganic contaminants removal from water with biochar, a renewable, low cost and sustainable adsorbent-a critical review, Bioresour. Technol. 160 (2014) 191–202, https://doi.org/10.1016/j.biortech.2014.01.120.

[14] Y. Dai, N. Zhang, C. Xing, Q. Cui, Q. Sun, The adsorption, regeneration and engineering applications of biochar for removal organic pollutants: a review, Chemosphere 223 (2019) 12–27, https://doi.org/10.1016/j.chemosphere.2019.01.161.

[15] A. Nasrullah, A.H. Bhat, A. Naeem, et al., High surface area mesoporous activated carbon-alginate beads for efficient removal of methylene blue, Int. J. Biol. Macromol. 107 (2018) 1792–1799, https://doi.org/10.1016/j.ijbiomac.2017.10.045.

[16] M.J. Ahmed, P.U. Okoye, E.H. Hummadi, B.H. Hameed, High-performance porous biochar from the pyrolysis of natural and renewable seaweed (Gelidiella acerosa) and its application for the adsorption of methylene blue, Bioresour. Technol. 278 (2019) 159–164, https://doi.org/10.1016/j.biortech.2019.01.054.

[17] A.A. Babaei, S.N. Alavi, M. Akbarifar, K. Ahmadi, A. Ramazanpour Esfahani, B. Kakavandi, Experimental and modeling study on adsorption of cationic methylene blue dye onto mesoporous biochars prepared from agrowaste, Desalination Water Treat. 57 (2016) 27199–27212, https://doi.org/10.1080/19443994.2016.1163736.

[18] J. Chen, C. Tang, X. Li, J. Sun, Y. Liu, W. Huang, A. Wang, Y. Lu, Preparation and modification of rape straw biochar and its adsorption characteristics for methylene blue in water, Water 14 (2022), https://doi.org/10.3390/w14223761.

[19] S. Fan, Y. Wang, Z. Wang, J. Tang, J. Tang, X. Li, Removal of methylene blue from aqueous solution by sewage sludge-derived biochar: adsorption kinetics, equilibrium, thermodynamics and mechanism, J. Environ. Chem. Eng. 5 (2017) 601–611, https://doi.org/10.1016/j.jece.2016.12.019.

[20] A.A.H. Saeed, N.Y. Harun, S. Sufian, A.A. Siyal, M. Zulfiqar, M.R. Bilad, A. Vagananthan, A. Al-Fakih, A.A.S. Ghaleb, N. Almahbashi, Eucheuma cottonii seaweed-based biochar for adsorption of methylene blue dye, Sustainability 12 (2020), https://doi.org/10.3390/su122410318.

[21] R. Liu, G. Liu, B. Yousaf, Z. Niu, Q. Abbas, Novel investigation of pyrolysis mechanisms and kinetics for functional groups in biomass matrix, Renew. Sustain. Energy Rev. 153 (2022), https://doi.org/10.1016/j.rser.2021.111761.

[22] S. Liu, J. Li, S. Xu, M. Wang, Y. Zhang, X. Xue, A modified method for enhancing adsorption capability of banana pseudostem biochar towards methylene blue at low temperature, Bioresour. Technol. 282 (2019) 48–55, https://doi.org/10.1016/j.biortech.2019.02.092.

[23] Y. Zhang, Y. Zheng, Y. Yang, J. Huang, A.R. Zimmerman, H. Chen, X. Hu, B. Gao, Mechanisms and adsorption capacities of hydrogen peroxide modified ball milled biochar for the removal of methylene blue from aqueous solutions, Bioresour. Technol. 337 (2021) 125432, https://doi.org/10.1016/j.biortech.2021.125432.

[24] A. Nasrullah, A.H. Bhat, M.H. Isa, et al., Efficient removal of methylene blue dye using mangosteen peel waste: kinetics, isotherms and artificial neural network (ANN) modeling, Desalination Water Treat. 86 (9410266) (2017) 191–202, https://doi.org/10.5004/dwt.2017.21295.

[25] N. Arumugam, S. Chelliapan, H. Kamyab, S. Thirugnana, N. Othman, N.S. Nasri, Treatment of wastewater using seaweed: a review, Int. J. Environ. Res. Publ. Health 15 (2018), https://doi.org/10.3390/ijerph15122851.

[26] S. El Atouani, Z. Belattmania, A. Reani, S. Tahiri, A. Aarfane, F. Bentiss, C. Jama, R. Zrid, B. Sabour, Brown seaweed sargassum muticum as low-cost biosorbent of methylene blue, Int. J. Environ. Res. 13 (2018) 131–142, https://doi.org/10.1007/s41742-018-0161-4.

[27] K. Marungrueng, P. Pavasant, High performance biosorbent (Caulerpa lentillifera) for basic dye removal, Bioresour. Technol. 98 (2007) 1567–1572, https://doi.org/10.1016/j.biortech.2006.06.010.

[28] Y.T. Li, B.J. Chen, W.D. Wu, K. Ge, X.Y. Wei, L.M. Kong, Y.Y. Xie, J.P. Gu, J.C. Zhang, T. Zhou, Antioxidant and antimicrobial evaluation of carboxymethylated and hydroxamated degraded polysaccharides from Sargassum fusiforme, Int. J. Biol. Macromol. 118 (2018) 1550–1557, https://doi.org/10.1016/j.ijbiomac.2018.06.196.

[29] R. Jiang, J. Tian, H. Zheng, J. Qi, S. Sun, X. Li, A novel magnetic adsorbent based on waste litchi peels for removing Pb(II) from aqueous solution, J. Environ. Manag. 155 (2015) 24–30, https://doi.org/10.1016/j.jenvman.2015.03.009.

[30] H. Dai, Y. Chen, L. Ma, Y. Zhang, B. Cui, Direct regeneration of hydrogels based on lemon peel and its isolated microcrystalline cellulose: characterization and application for methylene blue adsorption, Int. J. Biol. Macromol. 191 (2021) 129–138, https://doi.org/10.1016/j.ijbiomac.2021.09.063.

[31] X. Han, W. Wang, X. Ma, Adsorption characteristics of methylene blue onto low cost biomass material lotus leaf, Chem. Eng. J. 171 (2011) 1–8, https://doi.org/10.1016/j.cej.2011.02.067.

[32] B. Poornima, K.V.S.R.G. Prasad, K. Bharathi, Solid-state screening and evaluation of pioglitazone hydrochloride, Curr. Pharmaceut. Anal. 14 (2017), https://doi.org/10.2174/1573412913666161230160413.

[33] S.S. Kim, S.J. Kim, Y.D. Moon, Y.M. Leem, Thermal characteristics of chitin and hydroxypropyl chitin, Polymer 35 (15) (1994) 3212–3216, https://doi.org/10.1016/0032-3861(94)90124-4.

[34] R. Han, L. Zhang, C. Song, M. Zhang, H. Zhu, L. Zhang, Characterization of modified wheat straw, kinetic and equilibrium study about copper ion and methylene blue adsorption in batch mode, Carbohydr. Polym. 79 (2010) 1140–1149, https://doi.org/10.1016/j.carbpol.2009.10.054.

[35] S.S. Baral, N. Das, G. Roy Chaudhury, S.N. Das, A preliminary study on the adsorptive removal of Cr(VI) using seaweed, Hydrilla verticillata, J. Hazard Mater. 171 (2009) 358–369, https://doi.org/10.1016/j.jhazmat.2009.06.011.

[36] M. Yadav, S. Thakore, R. Jadeja, Removal of organic dyes using Fucus vesiculosus seaweed bioadsorbent an ecofriendly approach: equilibrium, kinetics and thermodynamic studies, Environmental Chemistry and Ecotoxicology 4 (2022) 67–77, https://doi.org/10.1016/j.enceco.2021.12.003.

[37] L. Chen, Y. Zhu, Y. Cui, R. Dai, Z. Shan, H. Chen, Fabrication of starch-based high-performance adsorptive hydrogels using a novel effective pretreatment and adsorption for cationic methylene blue dye: behavior and mechanism, Chem. Eng. J. 405 (2021), https://doi.org/10.1016/j.cej.2020.126953.

[38] M.S. Abubakar, B. Usman, Investigation of corrosion inhibition potential of ethanol extract of Balanites aegyptiaca leaves on mild steel in 1 m hydrochloric acid solution, Moroc. J. Chem. 7 (1) (2019) 82–97, https://doi.org/10.48317/IMIST.PRSM/morjchem-v7i1.14889, 7-1 (2019).

[39] A.A. Inyinbor, F.A. Adekola, G.A. Olatunji, Adsorption of Rhodamine B dye from aqueous solution on Irvingia gabonensis biomass: kinetics and thermodynamics studies, S. Afr. J. Chem. 68 (2015), https://doi.org/10.17159/0379-4350/2015/v68a17.

[40] N.M. Mahmoodi, B. Hayati, M. Arami, C. Lan, Adsorption of textile dyes on Pine Cone from colored wastewater: kinetic, equilibrium and thermodynamic studies, Desalination 268 (2011) 117–125, https://doi.org/10.1016/j.desal.2010.10.007.

[41] H. Abou Oualid, Y. Abdellaoui, M. Laabd, M. El Ouardi, Y. Brahmi, M. Iazza, J. Abou Oualid, Eco-efficient green seaweed Codium decorticatum biosorbent for textile dyes: characterization, mechanism, recyclability, and RSM optimization, ACS Omega 5 (2020) 22192–22207, https://doi.org/10.1021/acsomega.0c02311.

[42] M.H. Kanani-Jazi, S. Akbari, Optimization of Methylene Blue Dye Batch Adsorption by Carboxylic Acid Functionalized Halloysite Nanotubes, Eco-Friendly and Smart Polymer Systems, Springer International Publishing, 2020, pp. 220–223, https://doi.org/10.1007/978-3-030-45085-4_53.

[43] H. Zeng, W. Qi, L. Zhai, F. Wang, J. Zhang, D. Li, Magnetic biochar synthesized with waterworks sludge and sewage sludge and its potential for methylene blue removal, J. Environ. Chem. Eng. 9 (2021), https://doi.org/10.1016/j.jece.2021.105951.

[44] A.S. Khan, Z. Man, M.A. Bustam, et al., Kinetics and thermodynamic parameters of ionic liquid pretreated rubber wood biomass, J. Mol. Liq. 223 (2016) 754–762, https://doi.org/10.1016/j.molliq.2016.09.012.

[45] B.K. Nandi, A. Goswami, M.K. Purkait, Adsorption characteristics of brilliant green dye on kaolin, J. Hazard Mater. 161 (2009) 387–395, https://doi.org/10.1016/j.jhazmat.2008.03.110.
[46] N. Fiol, I. Villaescusa, Determination of sorbent point zero charge: usefulness in sorption studies, Environ. Chem. Lett. 7 (2008) 79–84, https://doi.org/10.1007/s10311-008-0139-0.
[47] B.C. Melo, F.A.A. Paulino, V.A. Cardoso, A.G.B. Pereira, A.R. Fajardo, F.H.A. Rodrigues, Cellulose nanowhiskers improve the methylene blue adsorption capacity of chitosan-g-poly(acrylic acid) hydrogel, Carbohydr. Polym. 181 (2018) 358–367, https://doi.org/10.1016/j.carbpol.2017.10.079.
[48] L. Wang, J. Zhang, A. Wang, Removal of methylene blue from aqueous solution using chitosan-g-poly(acrylic acid)/montmorillonite superadsorbent nanocomposite, Colloid Surf. A-Physicochem. Eng. Asp. 322 (2008) 47–53, https://doi.org/10.1016/j.colsurfa.2008.02.019.
[49] M. Uğurlu, Adsorption of a textile dye onto activated sepiolite, Microporous Mesoporous Mater. 119 (2009) 276–283, https://doi.org/10.1016/j.micromeso.2008.10.024.
[50] M. Das, M. Yadav, F. Shukla, S. Ansari, R.N. Jadeja, S. Thakore, Facile design of a dextran derived polyurethane hydrogel and metallopolymer: a sustainable approach for elimination of organic dyes and reduction of nitrophenols, New J. Chem. 44 (2020) 19122–19134, https://doi.org/10.1039/D0NJ01871F.
[51] A. Khaled, A. El Nemr, A. El-Sikaily, O. Abdelwahab, Removal of Direct N Blue-106 from artificial textile dye effluent using activated carbon from orange peel: adsorption isotherm and kinetic studies, J. Hazard Mater. 165 (2009) 100–110, https://doi.org/10.1016/j.jhazmat.2008.09.122.
[52] L. Abramian, H. El-Rassy, Adsorption kinetics and thermodynamics of azo-dye Orange II onto highly porous titania aerogel, Chem. Eng. J. 150 (2009) 403–410, https://doi.org/10.1016/j.cej.2009.01.019.
[53] I.A. Tan, A.L. Ahmad, B.H. Hameed, Adsorption of basic dye on high-surface-area activated carbon prepared from coconut husk: equilibrium, kinetic and thermodynamic studies, J. Hazard Mater. 154 (2008) 337–346, https://doi.org/10.1016/j.jhazmat.2007.10.031.
[54] G. Annadurai, L.Y. Ling, J.F. Lee, Adsorption of reactive dye from an aqueous solution by chitosan: isotherm, kinetic and thermodynamic analysis, J. Hazard Mater. 152 (2008) 337–346, https://doi.org/10.1016/j.jhazmat.2007.07.002.
[55] Y. Aldegs, M. Elbarghouthi, A. Elsheikh, G. Walker, Effect of solution pH, ionic strength, and temperature on adsorption behavior of reactive dyes on activated carbon, Dyes Pigments 77 (2008) 16–23, https://doi.org/10.1016/j.dyepig.2007.03.001.
[56] J. Feng, H. Ding, G. Yang, R. Wang, S. Li, J. Liao, Z. Li, D. Chen, Preparation of black-pearl reduced graphene oxide-sodium alginate hydrogel microspheres for adsorbing organic pollutants, J. Colloid Interface Sci. 508 (2017) 387–395, https://doi.org/10.1016/j.jcis.2017.07.113.
[57] X.-S. Hu, R. Liang, G. Sun, Super-adsorbent hydrogel for removal of methylene blue dye from aqueous solution, J. Mater. Chem. A 6 (2018) 17612–17624, https://doi.org/10.1039/C8TA04722G.